

RSC Advances



This is an *Accepted Manuscript*, which has been through the Royal Society of Chemistry peer review process and has been accepted for publication.

Accepted Manuscripts are published online shortly after acceptance, before technical editing, formatting and proof reading. Using this free service, authors can make their results available to the community, in citable form, before we publish the edited article. This *Accepted Manuscript* will be replaced by the edited, formatted and paginated article as soon as this is available.

You can find more information about *Accepted Manuscripts* in the [Information for Authors](#).

Please note that technical editing may introduce minor changes to the text and/or graphics, which may alter content. The journal's standard [Terms & Conditions](#) and the [Ethical guidelines](#) still apply. In no event shall the Royal Society of Chemistry be held responsible for any errors or omissions in this *Accepted Manuscript* or any consequences arising from the use of any information it contains.

ARTICLE

Soluble Bipolar Star-Shaped Molecule as Highly Stable and Efficient Blue Light Emitter

Cite this: DOI: 10.1039/x0xx00000x

Xuehan He,^a Lei Chen,^b Yongbiao Zhao,^c Siu Choon Ng,^d Xizu Wang,^e Xiaowei Sun,^c and Xiao 'Matthew' Hu^{*a}

Received 00th January 2012,
Accepted 00th January 2012

DOI: 10.1039/x0xx00000x

www.rsc.org/

A star-shaped blue small-molecule 1,3,5-tris(5-(4-(3,6-di-tert-butylcarbazol-9-yl)phenyl)-1,3,4-oxadiazol-2-yl)benzene (S-Cz-OXD) with donor- π -acceptor (D- π -A) structure was designed and synthesized by incorporating three (3,6-di-tert-butyl-9H-carbazol-9-yl)phenyl arms into an tris(1,3,4-oxadiazole)phenylene core. It gives pure blue photoluminescence emission at 424 nm with high quantum efficiency (Φ_f) (93%) in dilute toluene and has good solubility in common solvents. This star-shaped molecule also demonstrates enhanced Φ_f (72%) in film state. Moreover, the spectral stability of S-Cz-OXD is also excellent due to its low lying HOMO level and absence of fluorine moiety. The PL spectrum of S-Cz-OXD remains virtually unchanged even after annealing at 150 °C for 220 hours in air. Solution-processed non-doped electroluminescent device shows a low turn-on voltage of 3.7 V although there exists big energy barrier due to the bipolar design. The device emits stable pure blue light, CIE (Commission Internationale de L'Eclairage) coordinates of (0.16, 0.16) with high current efficiency (CE) and external quantum efficiency (EQE) of 4.22 cd A⁻¹ and 3.37% respectively. Mechanistic discussion is also carried out in relation to the molecular structure.

KEYWORDS: Organic semiconductor, Star-shaped bipolar molecule, Light emitting diode, Blue emission

1. Introduction

Solution-processed organic light-emitting diodes (OLEDs) is the most promising technology for low cost, flexible, large area full-color displays and solid state illuminations.^{1,2} As one of the three-primary colors, blue emitters could also act as the host material for green and red emitters to realize full-visible-spectra emission. Therefore, it is important to develop highly efficient, solution processable, stable and color-pure blue emitting materials.³

Due to their highly branched and globular features, star-shaped molecules could effectively suppress the intermolecular interaction in film state, leading to unique properties, such as enhanced solid-state luminescence, good film forming ability and excellent thermal stability.⁴⁻⁷ Therefore, star-shaped molecular design strategy is an effective way to improve the EL performance of OLEDs. For instance, Luo et al first reported a series of blue oligomers and polymers using truxene as the core and fluorene derivatives as the repeat unit of arms. They show improved EL efficiency with an EQE value of 2.9%,⁸ which is higher than that of linear polyfluorene (around 1.0%).⁹ Lai et al developed a set of fluorene-based six-armed nanostar macromolecules¹⁰ with greatly improved solid-state fluorescence quantum efficiency (around 90%) compared to

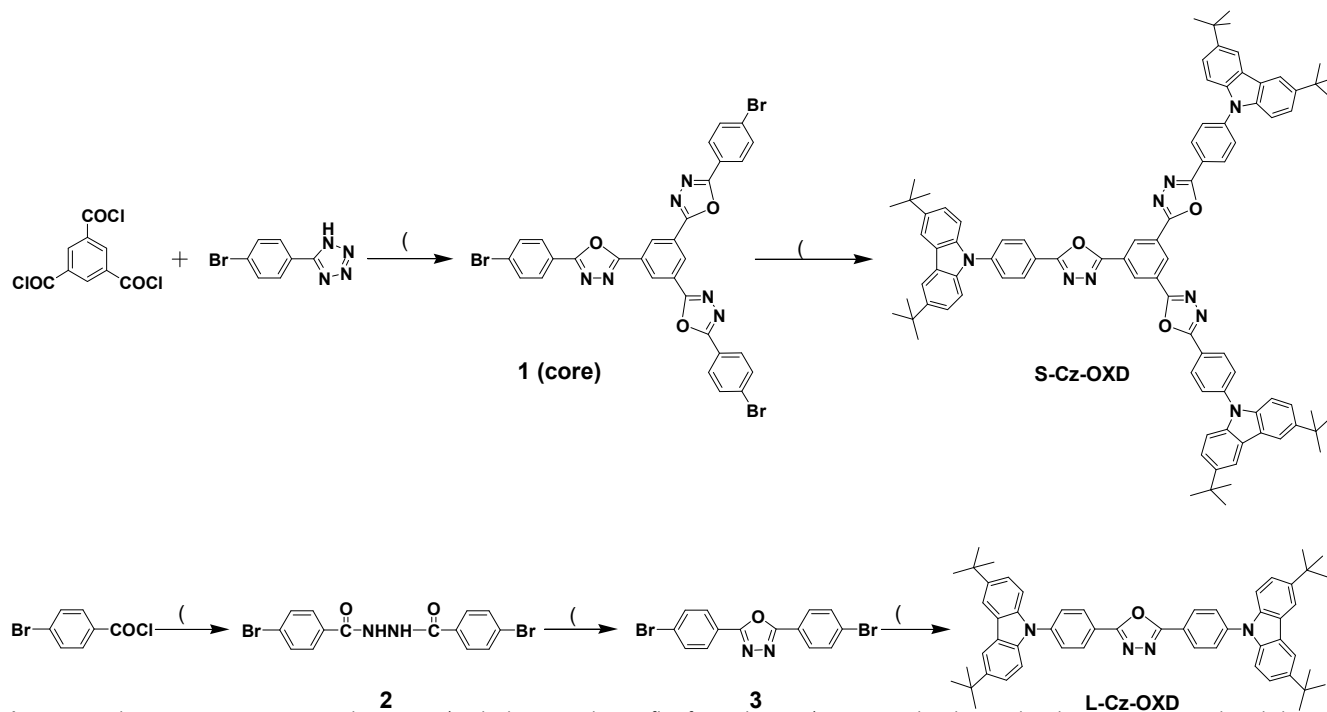
that of linear polyfluorene (55%).¹¹ Using a planar triphenylamine core, Yang et al designed a series of starburst fluorene oligomers with a maximum CE of 3.83 cd A⁻¹ and a maximum EQE of 4.9%.¹² Zou et al also reported a series of starburst oligofluorenes using phenyl as the core with a maximum EQE of 6.8% and CE of 5.4 cd A⁻¹.⁷ Subsequently, they fine-tuned the turn-on voltage at 3.6 V by introducing electron donor diphenylamine end-caps to raise the HOMO level although this may reduce the spectral stability.¹³ Improved device performance was also reported in star-like branched polyfluorene,^{14,15} even though polymers tend to have more batch to batch difference in average molecular weight and polydispersity, structural defects and more tedious procedures in removing residue catalysts.

Although numerous star-like blue oligomers/polymers were reported with good device efficiency, some issues remain hindering their practical application. Firstly, most of the reported materials were fluorene-based molecules showing good solubility and high PL quantum efficiency. However, fluorine has an intrinsic drawback of unstable EL spectrum. An additional green emission could be observed during long time operation or thermal treatment in air due to the generation of ketonic defects.¹⁶⁻¹⁹ Besides, more balanced carrier flow can be better achieved in a bipolar molecular design than that in

fluorine based materials which are strong p-type hole conductors. While, donor- π -Acceptor (D- π -A) push-pull design is usually used to improve the balance of charge transportation, few reported blue light emitting star-shaped molecules with D- π -A structures because the push-pull structure usually leads to lower band-gap and red-shift of the spectra.^{20,21} Jose et al synthesized two interesting blue light emitting D- π -A bipolar starburst molecules, but no device data were reported.²²

Based on the above consideration, we designed a solution processable star-shaped small-molecule with high PL efficiency, excellent spectra stability and bipolar characteristics by (1) utilizing carefully selected non-fluorene based building blocks with high stability; (2) introducing D- π -A pairs into

starburst structure while ensuring blue light emission. The target molecule 1,3,5-tris(5-(4-(3,6-di-tert-butylcarbazol-9-yl)phenyl)-1,3,4-oxadiazol-2-yl)benzene (S-Cz-OXD) comprising of tris(1,3,4-oxadiazole) phenylene (OXD) electron acceptor and 3,6-di-tert-butyl carbazole (*t*-BCz) electron donor (See **Scheme 1**). This molecule is readily synthesized and purified, and exhibits very high PL quantum efficiency. Furthermore, the cast film of S-Cz-OXD shows outstanding oxidation resistance and spectra stability. Non-doped device based on S-Cz-OXD show pure blue emission with a high efficiencies of 4.22 cd A⁻¹, an EQE of 3.37% and CIE coordinates of (0.16, 0.16).



Scheme 1 Synthesis route to S-Cz-OXD and L-Cz-OXD. i) anhydrous pyridine; reflux for 24 hours. ii) 3,6-Di-tert-butyl-9H-carbazole, CuI, K₂CO₃, 1,3-dimethyl-3,4,5,6-tetrahydro-2(1H)-pyrimidinone (DMPU), and 18-crown-6; 170 °C for 48 hours. iii) H₂NNH₂·H₂O, Et₃N, CH₂Cl₂; 40 °C for 2 hours. iv) SOCl₂, toluene; reflux for 12 hours.

2. Results and discussion

2.1. Molecular design and synthesis

The chemical structure of S-Cz-OXD is shown in **Scheme 1**. The electron-rich carbazole and electron-deficient oxadiazole units were selected because of their excellent charge transport properties and good chemical stability. Such a donor- π -acceptor structure renders the molecule bipolar characteristics which are favorable for more balanced charge injection and transport. For instance, adding an electron acceptor onto an oligofluorene was reported to substantially increase the device current efficiency.²³ On the other hand, D- π -A structures will lead to hole and electron traps on a same molecular and thus enhance the carrier recombination efficiency.²⁴ The three sterically hindered arms are designed to prevent aggregation and suppress fluorescence quenching, leading to high quantum efficiency.

Bulky *t*-butyl group on carbazole unit was introduced to improve the solubility and further suppress the molecular aggregation in solid state. For comparison, a linear analogue 2,5-bis(3,6-di-tert-butyl-carbazol-9-yl)phenyl-1,3,4-oxadiazole (L-Cz-OXD) (**Scheme 1**) was also synthesized and studied.

The synthesis route is also shown in **Scheme 1**. Intermediate 1 (the core) was synthesized by a cyclization reaction between 5-(4-Bromophenyl)-1H-tetrazole and 1,3,5-Benzenetricarboxylic acid chloride in dry pyridine.²⁵ Bis(4-bromobenzoyl)hydrazine (intermediate 2) and 2,5-Bis(4'-bromophenyl)-1,3,4-oxadiazole (intermediate 3) were synthesized according to literature.²⁶ S-Cz-OXD and L-Cz-OXD were obtained through an Ullmann reaction in the presence of CuI, K₂CO₃, 1,3-dimethyl-3,4,5,6-tetrahydro-2(1H)-pyrimidinone (DMPU), and 18-crown-6.²⁷ Their identity and purity were confirmed by ¹H NMR, ¹³C NMR spectra, MS (MALDI-TOF), and elemental analysis, as detailed in the

experimental part. S-Cz-OXD was checked to have good solubility. It could be dissolved no less than 30 mg mL⁻¹ in CHCl₃ and 15 mg mL⁻¹ in toluene or chlorobenzene. While, L-Cz-OXD just can be dissolved around 20mg mL⁻¹ in CHCl₃, and 5 mg mL⁻¹ in toluene or chlorobenzene under heating (60°C). The superior solubility of star-shaped molecules could be ascribed to the bulky steric structure impedes the aggregation of molecules in solution.

2.2. Properties and characterizations of the blue emitters

2.2.1. Photophysical properties

Figure 1a and **b** show the UV-visible absorption and PL spectra of S-Cz-OXD and L-Cz-OXD in both diluted toluene solution and film state, their corresponding peak emission wavelengths and Φ_f are listed in **Table 1**. The main absorption peaks of intramolecular charge transfer of S-Cz-OXD and L-Cz-OXD in diluted toluene are 369 nm and 360 nm, respectively. The peaks of PL emission wavelengths in solution are located at 422 nm for S-Cz-OXD and 397 nm for L-Cz-OXD. Both of them show very high PL quantum efficiency in dilute toluene solution, 93% for S-Cz-OXD, and 95% for L-Cz-OXD with 9,10-diphenylanthracene as reference.

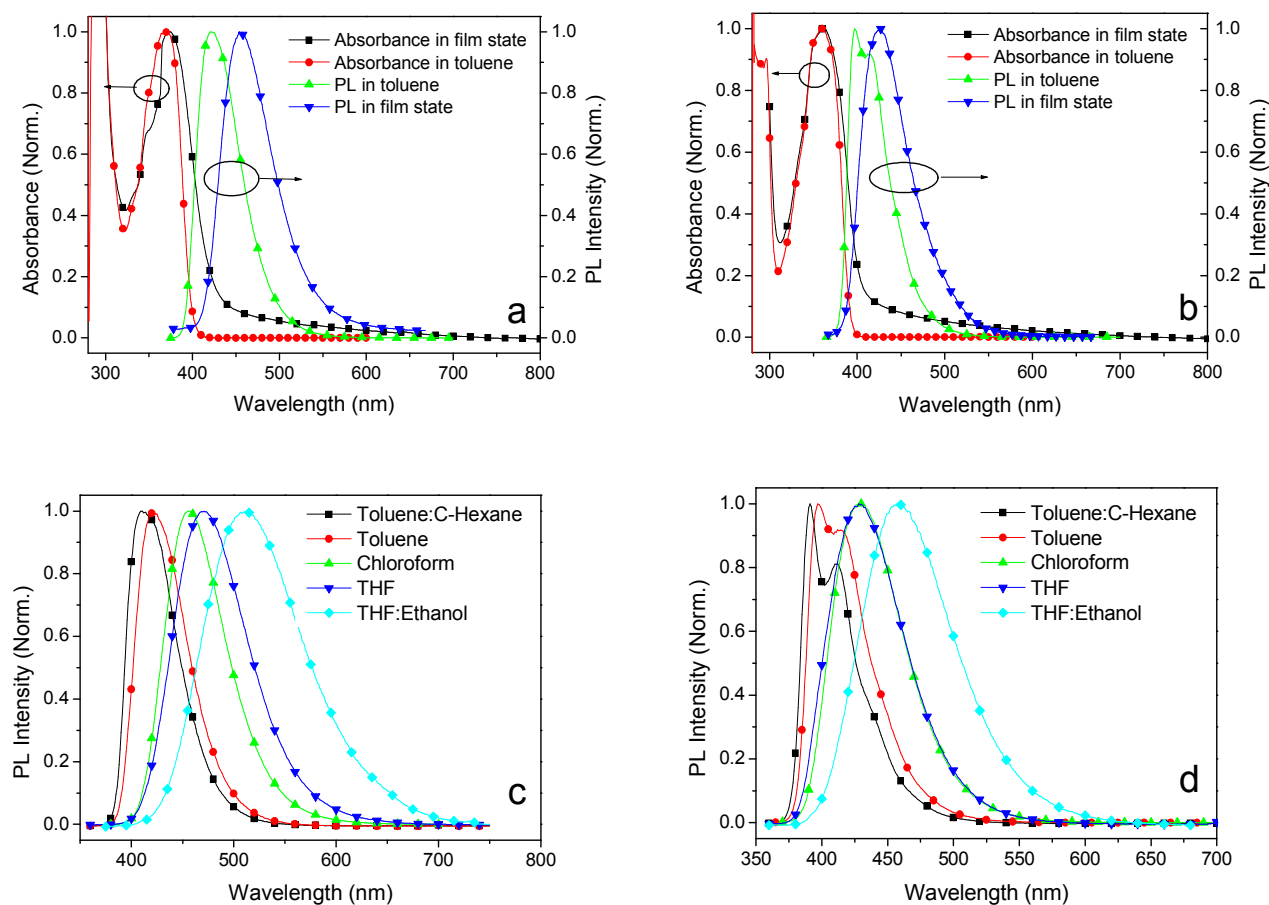


Figure 1. Absorption and PL spectra of (a) S-Cz-OXD and (b) L-Cz-OXD in dilute toluene solution and film state, and PL spectra of (c) S-Cz-OXD and (d) L-Cz-OXD in various solvents.

To study the condensed state optical properties, thin films of the molecules were prepared on quartz substrates by spin-coating from solutions followed by annealing at 150 °C for 30 minutes. The absorption peak of S-Cz-OXD and L-Cz-OXD show slightly red-shift to 372 nm and 362 nm in film state. The emission peaks of S-Cz-OXD and L-Cz-OXD exhibit obviously red-shifts to 455 nm and 425 nm, respectively. The solid-state PL quantum efficiency of these films were recorded by integrated sphere. S-Cz-OXD exhibits a quite high Φ_f value of 72% in solid-state, this value of L-Cz-OXD is only 47%,

indicating that S-Cz-OXD can effectively suppress the concentration quenching in film due to its highly branched structure.

Most molecules with donor-acceptor structure usually show bathochromic shift in polar solvent because the exciton could be more stabilized under polar surrounding. Therefore, we also studied the solvatochromism effect of our compounds by employing solvents with different polarities, including mixed solvent of toluene:cyclohexane (1:1, v/v), toluene, chloroform, THF, and mixed solvent of THF:ethanol (1:1, v/v). The reason

for using mixed solvent is that the solubility of L-Cz-OXD is too low to make PL measurement in individual cyclohexane and ethanol solvent. The resultant spectra are shown in **Figure 1, c** and **d**. It can be seen that with increased solvent polarity,

the maximum emission peaks show bathochromic shift from 411 nm to 511 nm for S-Cz-OXD and from 391 nm to 458 nm for L-Cz-OXD. Their emission peaks red-shift about 100 nm and 67 nm, respectively.

Table 1. Photophysical, electrochemical, and thermal properties of S-Cz-OXD and L-Cz-OXD

Compound	$\lambda_{\text{max}}^{\text{Abs}}$ (nm) [a]	$\lambda_{\text{max}}^{\text{PL}}$ (nm) [a]	Φ_{r} (%) [a]	$E_{\text{onset}}^{\text{oxd}}$ (V) [b]	$E_{\text{onset}}^{\text{red}}$ (V) [b]	E_{HOMO} (eV)	E_{LUMO} (eV)	E_{g} (eV)	T_{g} (°C)	T_{d} (°C)
S-Cz-OXD	369/372	422/455	93/72	1.26	-1.51	-5.66	-2.89	2.77	137	447
L-Cz-OXD	360/362	397/425	95/47	1.27	-1.58	-5.67	-2.82	2.85	141	423

[a] Measured in around 10^{-6} M toluene solution (former) and film (later) state; [b] Using 0.1 M $(\text{C}_4\text{H}_9)_4\text{NClO}_4$ in CH_2Cl_2 as supporting electrolyte, Ag/AgCl as reference electrode.

2.2.2. Electrochemical and thermal properties

Cyclic voltammetry measurement has been demonstrated to investigate the electrochemical properties of the blue emitters. The results are shown in **Figure 2**. S-Cz-OXD and L-Cz-OXD exhibited reversible redox behavior under both positive and negative drive bias, which can be attributed to the *t*-BCz donor units and the OXD acceptor core, respectively, indicating their distinct bipolar properties. Their highest occupied molecular orbital (HOMO) and lowest unoccupied molecular orbital (LUMO) energy levels are calculated from the onset oxidation and reduction potential according to the formula $E_{\text{HOMO}} = -e(E_{\text{onset}}^{\text{oxd}} + 4.4)$ (eV) and $E_{\text{LUMO}} = -e(E_{\text{onset}}^{\text{red}} + 4.4)$ (eV). All these data are listed in **Table 1**. The calculated HOMO energy levels are quite similar for S-Cz-OXD (-5.66 eV) and L-Cz-OXD (-5.67 eV), suggesting the electron-donating ability of two compounds are almost the same. The calculated LUMO energy level of S-Cz-OXD is -2.89 eV, slightly deeper than that of L-Cz-OXD (-2.82 eV), declaring stronger electron-withdrawing ability for tris(1,3,4-oxadiazole)phenylene compared to the single 1,3,4-oxadiazole unit. The calculated energy bandgap for S-Cz-OXD is 2.77 eV, slightly lower than 2.85 eV for L-Cz-OXD. These findings are consistent with the PL measurement results. S-Cz-OXD displays longer emission wavelength in both solution and solid state as well as stronger solvatochromism effect. It should possess stronger intramolecular charge transfer effect. Considering the same HOMO level of the two compounds, it can be attributed to the deeper LUMO energy level of the tris(1,3,4-oxadiazole)phenylene core.

temperature (T_{d} , 5% weight loss) is 447 °C and 423 °C, and the distinct glass transition temperature (T_{g}) is 137 °C and 141 °C for S-Cz-OXD and L-Cz-OXD, respectively. The high T_{d} and T_{g} temperatures further guarantee the thermal stability during practical application.

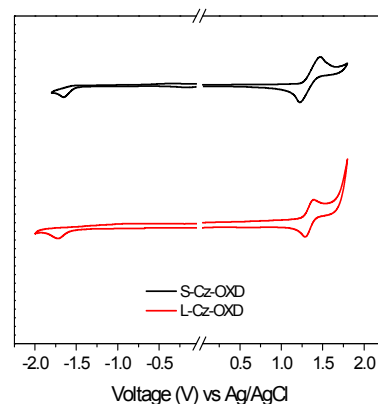
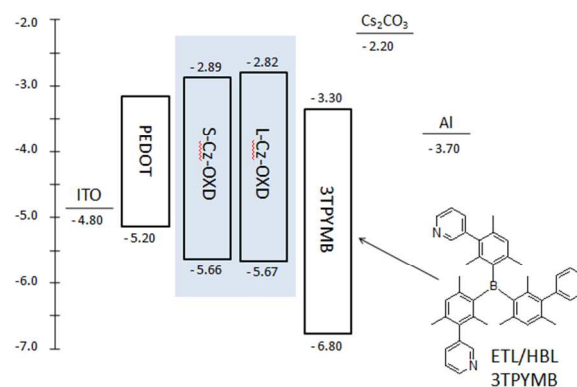


Figure 2. Cyclic voltammograms of S-Cz-OXD and L-Cz-OXD

2.3. Electroluminescent properties of non-doped devices



Scheme 2. Energy level diagram of the OLED devices and molecular structure of 3TPYMB

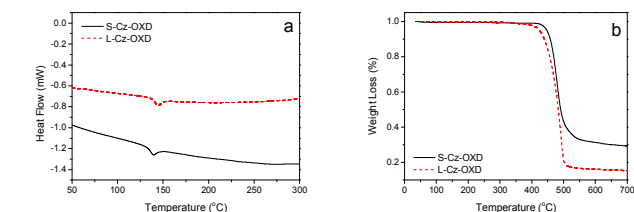


Figure 3. (a) DSC traces and (b) TGA thermogram of S-Cz-OXD and L-Cz-OXD

The thermal properties of S-Cz-OXD and L-Cz-OXD were explored by thermogravimetric analysis (TGA) and differential scanning calorimetry (DSC) measurement as shown in **Figure 3**. The results are also listed in **Table 1**. The decomposition

To investigate the EL properties of S-Cz-OXD, non-doped devices with configurations of ITO/PEDOT:PSS/S-Cz-OXD/3TPYMB/ Cs_2CO_3 /Al was fabricated. Here, PEDOT:PSS

is Poly(3,4-ethylenedioxythiophene) Polystyrene sulfonate. 3TPYMB is tris(2,4,6-trimethyl-3-(pyridin-3-yl)phenyl)borane, serving as both electron transporting and hole blocking materials. Control device using L-Cz-OXD as the emitting

layer were also fabricated for comparison. The energy diagram of the devices and the chemical structure of 3TPYMB were shown in **Scheme 2**.

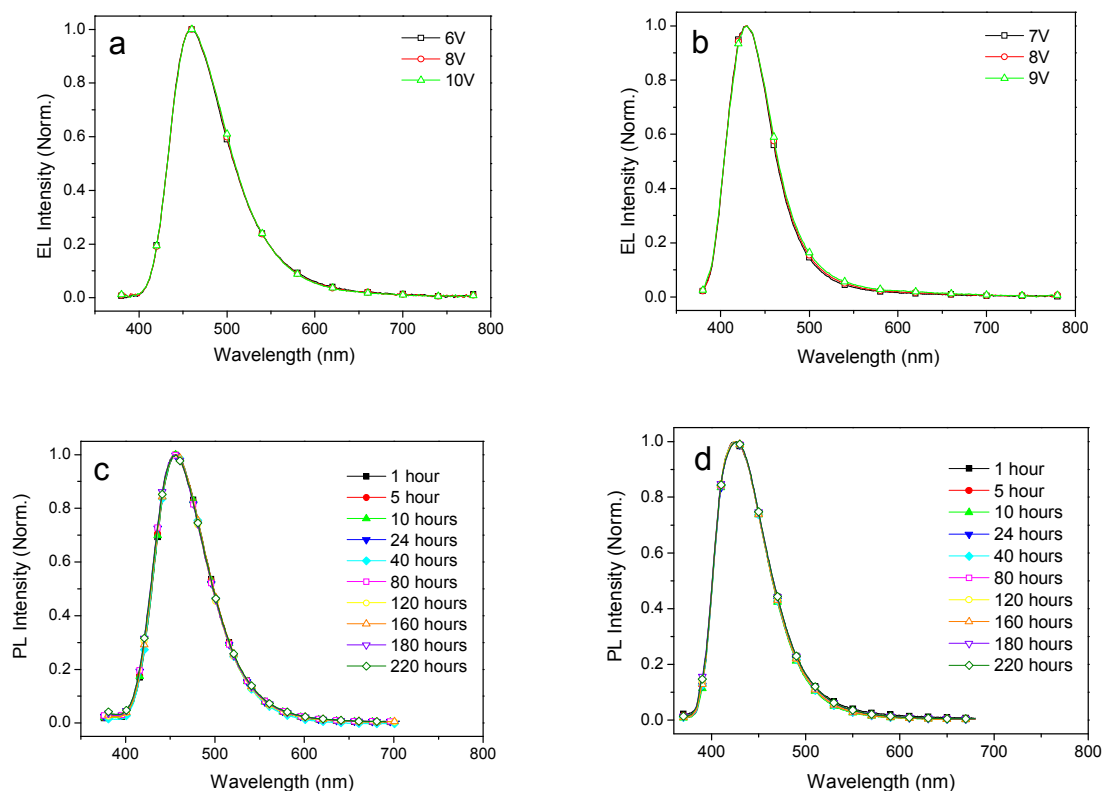


Figure 4. Normalized EL spectra of devices based on (a) S-Cz-OXD and (b) L-Cz-OXD at different applied voltages, and PL spectra of (c) S-Cz-OXD and (d) L-Cz-OXD during heating process at 150 °C in ambient air

The electroluminescent (EL) spectra of the devices at different applied voltages could be observed in **Figure 4, a** and **b**. The common way to reduce the turn-on voltage is to increase the HOMO level of the material to get a narrow energy barrier (usually PEDOT:PSS for solution processing OLED device).¹³ In our case, although there exists large hole injection barrier from PEDOT:PSS layer (-5.2 eV) to the HOMO level of emitting layer (-5.66 eV and -5.67 eV), both devices show low turn-on voltages especially the one based on S-Cz-OXD has a turn-on voltage at 3.7 V. This can be ascribed to its bipolar structure with good hole/electron transporting properties. Pure and deep blue emission peaking at 459nm and 429nm were obtained for device based on S-Cz-OXD and L-Cz-OXD. They are nearly identical with the corresponding PL spectra of the films with only a little red-shift. The CIE coordinates of the devices are demonstrated to be (0.16, 0.16), (0.16, 0.07), as shown in **Table 2**. Moreover, no significant change in the EL spectra was observed at various driving voltages, indicating an excellent voltage-independent and stable EL spectrum.

As mentioned above, one of the serious problems for fluorene-based materials is the unstable EL spectrum arising from the generation of fluorenone defects. It can be verified

from the additional green emission band in PL spectrum after thermal treatment under high temperature in air.²⁸ In order to investigate the emissive stability of S-Cz-OXD and L-Cz-OXD, the PL spectra of their solution-casted films were recorded after different durations of heat treatment at 150 °C in ambient condition (**Figure 4, c** and **d**). It could be observed that there is almost no change of the PL spectra even after 220 hours thermal treatment. The excellent spectra stability of S-Cz-OXD and L-Cz-OXD is a greatly improvement compared to those fluorine-based organic light emitting materials. We believe that this is due to the high stability of building-blocks such as carbazole and oxadiazole as well as very low lying HOMO energy level at -5.66 eV resulting in excellent the oxidative stability.

Figure 5 illustrates the detailed performances of the non-doped device based on the blue emitters. The electroluminescent performances were outlined in **Table 2**. The devices of S-Cz-OXD show high EL performances. It can reach a maximum luminance of 3601 cd m⁻², a maximum CE of 4.22 cd A⁻¹, an EQE of 3.37%, and a PE of 2.60 lm W⁻¹. It still remains the efficiency as high as of 3.44 cd A⁻¹ and an EQE of 2.48% at the brightness of 1000 cd m⁻². However, the control

device of L-Cz-OXD exhibits much poorer EL performance, with a maximum brightness of 295 cd m^{-2} , a CE of 0.62 cd A^{-1} , an EQE of 1.68% and a PE of 0.38 lm W^{-1} . The inferior

performance could be ascribed to the low solid-state PL efficiency, poor solubility and inferior film formation ability.

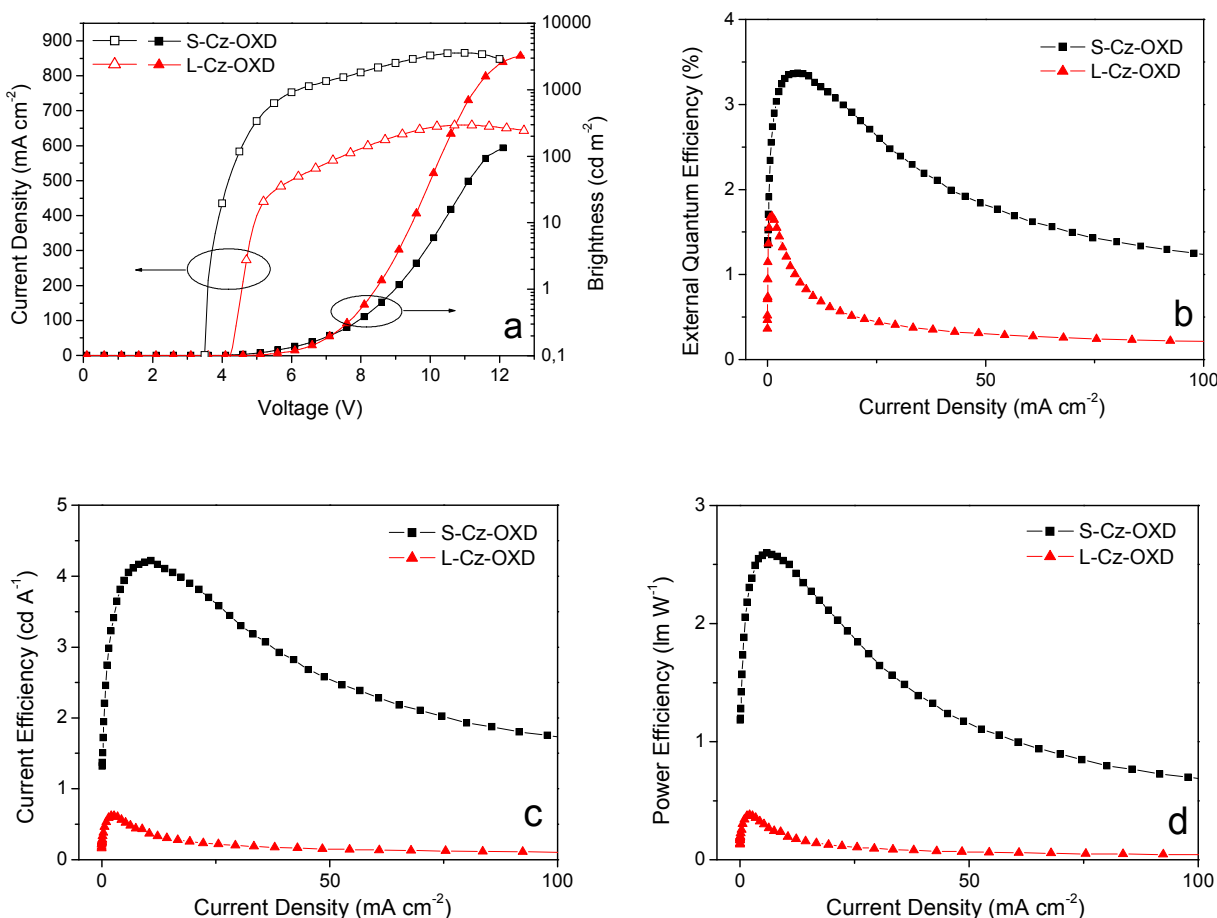


Figure 5.(a) Current density–voltage and brightness–voltage spectra of devices; (b) Current efficiency versus current density of devices; (c) Power efficiency versus current density of devices; (d) External quantum efficiency versus current density of devices.

Table 2.Electroluminescence characteristics of the devices based on S-Cz-OXD and L-Cz-OXD

Device	V_{on} [a] (V)	Max Brightness (cd m^{-2})	EQE [b] (%)	CE [b] (cd A^{-1})	PE [b] (lm W^{-1})	λ_{max} (nm)	CIE (x, y)
S-Cz-OXD	3.7	3601	3.37 / 3.26 / 2.48	4.22 / 4.21 / 3.44	2.60 / 2.50 / 1.74	459	(0.16, 0.16)
L-Cz-OXD	4.2	295	1.68 / 0.36 / n.a.	0.62 / 0.39 / n.a.	0.38 / 0.18 / n.a.	429	(0.16, 0.07)

[a] Turn-on voltage at a brightness of 1 cd m^{-2} ; [b] Maximum value and estimated values at 100 cd m^{-2} and 1000 cd m^{-2}

3. Conclusion

In summary, we report a highly soluble star-shaped blue molecule S-Cz-OXD with bipolar feature. The unique branched molecular structure endows it superior film-forming ability, high PL efficiency in film state as well as good thermal stability. Furthermore, S-Cz-OXD demonstrates outstanding spectral stability under long-term heat treatment in air. As a result, efficient and stable blue electroluminescence based on S-Cz-OXD was realized with a current efficiency of 4.22 cd A^{-1} and an EQE of 3.37%. It is one of the best results for solution-

processed non-doped blue device based on fluorene-free materials, indicating its potential for practical applications.

Experimental Section

3.1. Materials and synthesis

Materials:

Chemical reagents were purchased from Aldrich, Acros or Scientific Resources Pte Ltd, and used as received without further purified. Anhydrous toluene and THF were obtained

through a solvent purification system. All manipulations involving air and water sensitive reagents were performed under an atmosphere of dry nitrogen. All glassware was dried in 120 °C oven for more than 2 hours before usage.

Synthesis:

Synthesis of the core (intermediate 1): 1, 3, 5-Tris(4-bromophenyl)-1,3,4-oxadiazol-2-yl)benzene

3.98 g of 5-(4-Bromophenyl)-1H-tetrazole (15 mmol) and 13.5 g of 1,3,5-Benzenetricarboxylic acid chloride (60 mmol) were mixed with 250 ml anhydrous pyridine in a 500 ml round bottom flask. The resulting mixture was refluxed in a nitrogen atmosphere for 24 hours. After cooled the reaction to ambient temperature, the solid product, collected by filtration, was washed repeatedly with methanol and water each three times to afford a gray powder with a yield of 75%. MS (MALDI-TOF, m/z): [M]⁺Calcd. For C₃₀H₁₅Br₃N₆O₃: 747.19. Found: 749.2. No NMR data was recorded for this compound because it is insoluble in organic solvents such as CHCl₃, THF, and DMSO.

Synthesis of S-Cz-OXD

5.0 g of 3,6-Di-tert-butyl-9H-carbazole (18 mmol), 2.3 g of intermediate 1 (3 mmol), 2.76 g of K₂CO₃ (20 mmol), 0.19 g of CuI (1 mmol), 1 ml of DMPU, and 0.09 g of 18-crown-6 (0.3 mmol) were added into a 150 ml round bottom flask followed by evacuated and backfilled with N₂. The mixture was stirred at 170 °C for 48 h. After cooling to room temperature, the mixture was dissolved with dichloromethane and washed with brine for several times. Then the solution was dried with anhydrous sodium sulfate. After filtration and removal of the solvent, the residue was purified by silica column chromatography followed by two times of recrystallization to give the S-Cz-OXD as a white solid (yield: 37%). ¹H NMR (CDCl₃, 500 MHz, δ): 1.49 (s, 54H), 7.49-7.53 (m, 12H), 7.86 (d, *J* = 8.5 Hz, 6H), 8.17 (d, *J* = 0.9 Hz, 6H), 8.48 (d, *J* = 8.5 Hz, 6H), 9.15 (s, 3H). ¹³C NMR (CDCl₃, 125 MHz, δ): 32.0, 34.8, 109.2, 116.5, 121.1, 123.9, 124.0, 126.3, 126.7, 127.3, 128.9, 138.5, 142.1, 143.8, 162.8, 165.1. MS (MALDI-TOF, m/z): [M]⁺Calcd. For C₉₀H₈₇N₉O₃: 1341.7. Found: 1339.19. Anal. Calcd. For C₉₀H₈₇N₉O₃: C, 80.51; H, 6.53; N, 9.39; O, 3.57. Found: C, 80.47; H, 6.56; N, 9.41; O, 3.53.

Synthesis of L-Cz-OXD

Similar procedures were used to synthesize L-Cz-OXD. 5.6 g of 3,6-Di-tert-butyl-9H-carbazole (20 mmol), 1.9 g of intermediate 3 (5 mmol), 2.76 g of K₂CO₃ (20 mmol), 0.19 g of CuI (2 mmol), 1 ml of DMPU, and 0.09 g of 18-crown-6 (0.3 mmol) were mixed and stirred at 170 °C for 48 h under a N₂ atmosphere. After purification and recrystallization, L-Cz-OXD white solid was obtained (yield: 60%). ¹H NMR (CDCl₃, 400 MHz, δ): 1.48 (s, 36H), 7.46-7.53 (m, 8H), 7.81 (d, *J* = 8.5 Hz, 4H), 8.16 (d, *J* = 1.3 Hz, 4H), 8.40 (d, *J* = 8.5 Hz, 4H). ¹³C NMR (CDCl₃, 400 MHz, δ): 29.9, 32.1, 35.0, 109.4, 116.6, 122.0, 124.1, 126.9, 128.7, 138.8, 141.8, 143.9, 164.4. MS (MALDI-TOF, m/z): [M]⁺Calcd. For C₅₄H₅₆N₄O: 776.5.

Found: 774.4. Anal. Calcd. For C₅₄H₅₆N₄O: C, 83.47; H, 7.26; N, 7.21; O, 2.06. Found: C, 83.44; H, 7.29; N, 7.15; O, 2.08.

3.2. Measurement and instruments

¹H and ¹³C nuclear magnetic resonance (NMR) spectra were collected on a Bruker DRX spectrometer operating at 400 MHz using deuterated chloroform as solvent with tetramethylsilane (TMS) as reference. Elemental analyses were carried out on ElementarVario EL. Molecular weight was determined using Matrix assisted laser desorption ionization/Time-of-flight (MALDI-TOF, AXIMA Performance). Thermal analyses were carried out using differential scanning calorimetry (DSC, Q10 TA Instrument) and thermogravimetric analyses (TGA 2950, TA Instrument) at a heating rate of 10 °C min⁻¹. UV-visible absorption spectra and emission spectra were recorded on UV-Vis Spectrophotometer (Shimadzu UV-2501 PC) and Shimadzu RF 5301 Spectrofluorophotometer, respectively. Fluorescence quantum yields (Φ_f) of the samples both in THF solutions and as films were measured by using 9,10-diphenylanthracene ($\Phi_f = 0.92$ in toluene and $\Phi_f = 0.83$ dispersed in PMMA films with a concentration lower than 1×10^{-3} M) as standards. The concentrations of their dilute toluene solution were around 10⁻⁶ M with an absorbance lower than 0.05, while the thickness of films was around 70 nm. Quantum yield was calculated according to equation $\Phi_n = \Phi_s I_n A_s \eta_n^2 / A_n I_s \eta_s^2$ where Φ_n is the fluorescence quantum yield of the sample, Φ_s is the fluorescence quantum yield of the standard reference, I_n and I_s are the integrated emission intensities of the sample and the standard, respectively, A_n and A_s are the absorbance of the sample and the standard at the excitation wavelength, respectively, and η_n and η_s are the refractive indexes of the corresponding solutions. Cyclic voltammetry was carried out on a CHI660A electrochemical workstation at a scan rate of 100 mV s⁻¹ in a nitrogen-saturated solution of 0.1 M Tetrabutylammonium perchlorate ((C₄H₉)₄NClO₄) in anhydrous methylene chloride (CH₂Cl₂), using a glassy carbon electrode as working electrode, a Pt wire as counter electrode, and an Ag/AgCl electrode as reference electrode. The energy band gap was calculated from $E_g = E_{LUMO} - E_{HOMO}$ (eV).

3.3. Device fabrication and characterizations

Patterned ITO-coated glass (sheet resistance 10 Ω per square) was cleaned sequentially with detergent, de-ionized water, acetone and isopropanol, each for 20 min in an ultrasonic bath. Then the ITO substrates were blow-dried with nitrogen gas and undergo O₂ plasma cleaning for 10 min, PEDOT:PSS (4083) (30 nm) was spin-coated on the ITO substrate at 4000 rpm for 60 sec and then annealed for 15 min at 120 °C. Then emitting layer was spin coated on PEDOT:PSS layer from a 12 mg mL⁻¹ solution in a mixed solvent (1:1 v/v) of chloroform:chlorobenzene for 60 sec at 2500 rpm, and annealed at 120 °C for 30 min (70 nm). Then 3TPYMB (40 nm), Cs₂CO₃ (1 nm) and Al (120 nm) were successively evaporated on the emitting layer in a multi-source vacuum evaporator at a base pressure of 4 × 10⁻⁴ Pa. The evaporation rates and thickness

were monitored with several quartz crystals located above the crucibles. Calibration of the layer thickness was performed using a surface profilometer. Each patterned device has a 2 mm × 2 mm active area. Except for PEDOT deposition, all other fabrication processes were carried out in a glove box with less than 1 ppm oxygen and moisture. J-V and L-V data were collected using a source meter (Yokogawa GS610) and a luminance meter (Konica Minolta LS-110) with a customized Labview program. Electroluminescence (EL) spectra were recorded with a spectrometer (Photo Research PR705). The AC voltage used to drive the device for EL spectrum measurement was generated by the same sourcemeter operating in a pulse mode (rectangular shape, 50% duty cycle, 50 Hz).

Acknowledgements

Xuehan He and Lei Chen contributed equally to this work. The authors acknowledge the financial support from the research scholarship by Nanyang Technological University (NTU) in Singapore.

Notes and references

^aSchool of Materials Science and Engineering, Nanyang Technological University, Singapore 639798. E-mail: ASXHU@ntu.edu.sg

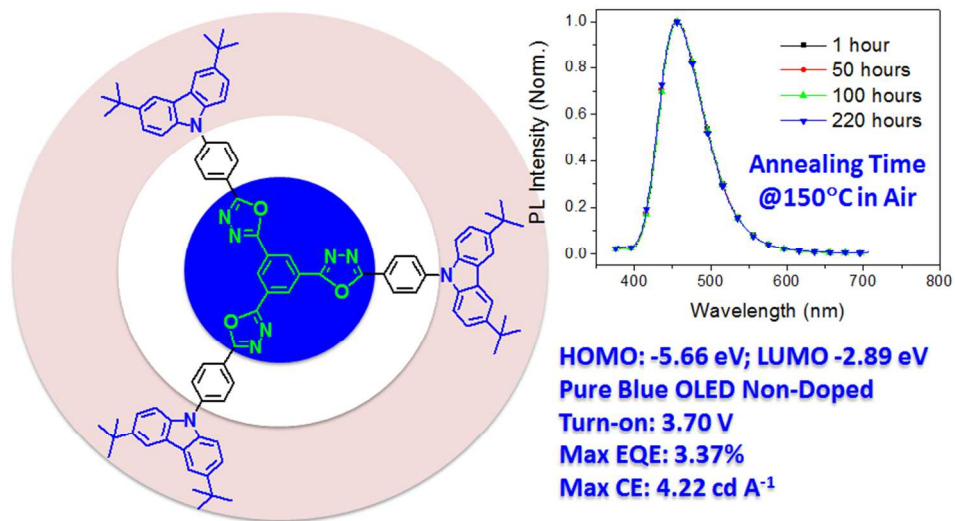
^bDepartment of Material Science and Engineering, National University of Singapore.

^cSchool of Electrical and Electronic Engineering, Nanyang Technological University.

^dSchool of Chemical and Biomedical Engineering, Nanyang Technological University.

^eInstitute of Materials Research and Engineering (IMRE), Singapore.

- C. Zhong, C. Duan, F. Huang, H. Wu, and Y. Cao, *Chem. Mater.*, 2011, **23**, 326–340.
- L. Duan, L. Hou, T.-W. Lee, J. Qiao, D. Zhang, G. Dong, L. Wang, and Y. Qiu, *J. Mater. Chem.*, 2010, **20**, 6392–6407.
- Y.-Y. Lyu, J. Kwak, O. Kwon, S.-H. Lee, D. Kim, C. Lee, and K. Char, *Adv. Mater.*, 2008, **20**, 2720–2729.
- W. Jiang, L. Duan, J. Qiao, D. Zhang, G. Dong, L. Wang, and Y. Qiu, *J. Mater. Chem.*, 2010, **20**, 6131–6137.
- Z. star-shaped host materials for highly efficient solution-processed phosphorescent organic light-emitting diodes Ge, T. Hayakawa, S. Ando, M. Ueda, T. Akiike, H. Miyamoto, T. Kajita, and M. Kakimoto, *Adv. Funct. Mater.*, 2008, **18**, 584–590.
- S. Ye, Y. Liu, K. Lu, W. Wu, C. Du, Y. Liu, H. Liu, T. Wu, and G. Yu, *Adv. Funct. Mater.*, 2010, **20**, 3125–3135.
- Y. Zou, J. Zou, T. Ye, H. Li, C. Yang, H. Wu, D. Ma, J. Qin, and Y. Cao, *Adv. Funct. Mater.*, 2013, **23**, 1781–1788.
- J. Luo, Y. Zhou, Z.-Q. Niu, Q.-F. Zhou, Y. Ma, and J. Pei, *J. Am. Chem. Soc.*, 2007, **129**, 11314–11315.
- D. Neher, *Macromol. Rapid Commun.*, 2001, **22**, 1365–1385.
- W.-Y. Lai, R. Xia, Q.-Y. He, P. a. Levermore, W. Huang, and D. D. C. Bradley, *Adv. Mater.*, 2009, **21**, 355–360.
- C. Chou, S. Hsu, K. Dinakaran, M. Chiu, and K. Wei, *Macromolecules*, 2005, **38**, 745–751.
- C. Liu, Y. Li, Y. Zhang, C. Yang, H. Wu, J. Qin, and Y. Cao, *Chem. - A Eur. J.*, 2012, **18**, 6928–34.
- C. Liu, Q. Fu, Y. Zou, C. Yang, and J. Qin, *Chem. Mater.*, 2014, **26**, 3074–3083.
- L. Chen, P. Li, H. Tong, Z. Xie, L. Wang, X. Jing, and F. Wang, *J. Polym. Sci. Part A Polym. Chem.*, 2012, **50**, 2854–2862.
- L. Chen, P. Li, Y. Cheng, Z. Xie, L. Wang, X. Jing, and F. Wang, *Adv. Mater.*, 2011, **23**, 2986–2990.
- M. Sims, D. D. C. Bradley, M. Ariu, M. Koeberg, A. Asimakis, M. Grell, and D. G. Lidzey, *Adv. Funct. Mater.*, 2004, **14**, 765–781.
- S. Y. Cho, A. C. Grimsdale, D. J. Jones, S. E. Watkins, and A. B. Holmes, *J. Am. Chem. Soc.*, 2007, **129**, 11910–11911.
- B. R. Abbel, M. Wolffs, R. A. A. Bovee, J. L. J. Van Dongen, X. Lou, O. Henze, W. J. Feast, E. W. Meijer, and A. P. H. J. Schenning, *Adv. Mater.*, 2009, **21**, 597–602.
- C. Li and Z. Bo, *Polymer (Guildf.)*, 2010, **51**, 4273–4294.
- Shijie Ren, Danli Zeng, Hongliang Zhong, Yaochuan Wang, Shixiong Qian, and Qiang Fang, *J. Phys. Chem. B*, 2010, **114**, 10374–10383.
- C. Coia, C. Ruiz, Á. L. Álvarez, S. Álvarez-García, E. M. García-Frutos, B. Gómez-Lor, and A. de Andrés, *Org. Electron.*, 2012, **13**, 2138–2148.
- J. Natera, L. Otero, F. D'Eramo, L. Sereno, F. Fungo, N.-S. Wang, Y.-M. Tsai, and K.-T. Wong, *Macromolecules*, 2009, **42**, 626–635.
- W. Li, D. Liu, F. Shen, D. Ma, Z. Wang, T. Feng, Y. Xu, B. Yang, and Y. Ma, *Adv. Funct. Mater.*, 2012, **22**, 2797–2803.
- B. Chen, J. Ding, L. Wang, X. Jing, and F. Wang, *Chem. Commun. (Camb.)*, 2012, **48**, 8970–8972.
- Sijian Hou and Wai Kin Chan, *Macromolecules*, 2002, **35**, 850–856.
- Dong-Cheol Shin, Jun-Hwan Ahn, Yun-Hi Kim, and S.-K. Kwon, *J. Polym. Sci. Part A Polym. Chem.*, 2000, **38**, 3086–3091.
- S. Ye, Y. Liu, J. Chen, K. Lu, W. Wu, C. Du, Y. Liu, T. Wu, Z. Shuai, and G. Yu, *Adv. Mater.*, 2010, **22**, 4167–4171.
- X. Guo, Y. Cheng, Z. Xie, Y. Geng, L. Wang, X. Jing, and F. Wang, *Macromol. Rapid Commun.*, 2009, **30**, 816–825.



258x144mm (96 x 96 DPI)